228 (2023) 212010

Contents lists available at ScienceDirect

Geoenergy Science and Engineering

journal homepage: www.sciencedirect.com/journal/geoenergy-science-and-engineering

Laboratory experiments and modelling of the geochemical interaction of a gabbro-anorthosite with seawater and supercritical CO_2: A mineral carbonation study

Edgar Berrezueta[a,*], Patrícia Moita[b,c], Jorge Pedro[b,d], Halidi Abdoulghafour[d], José Mirão[b,c], Massimo Beltrame[c], Pedro Barrulas[c], Alexandre Araújo[b,d], Maria Helena Caeiro[d], Lopes Luís[b,d], Júlio Carneiro[b,d]

[a] *Instituto Geológico y Minero de España (CN IGME, CSIC), C/Matemático Pedrayes 25, 33005, Oviedo, Spain*
[b] *Departamento de Geociências, Escola de Ciências e Tecnologia, Universidade de Évora, Rua Romão Ramalho, 59, 7000-671, Évora, Portugal*
[c] *Laboratório HERCULES, Universidade de Évora, Largo Marquês de Marialva, 8, 7000-809, Évora, Portugal*
[d] *Instituto de Ciências da Terra, Universidade de Évora, Rua Romão Ramalho, 59, 7000-671, Évora, Portugal*

ARTICLE INFO

Keywords:
CO_2 storage
Supercritical CO_2
Mafic plutonic rocks
Experimental test

ABSTRACT

The potential for mineral carbonation of carbon dioxide (CO_2) in a plutonic mafic rock is addressed in this work through a set of laboratory experiments on a gabbro-anorthosite sample from the Torrão - Odivelas Massif (Portugal). The experiment was conducted in two stages under pressure (8 MPa) and temperature (313.15 K) conditions similar to those expected around a CO_2 injection well. Stage-I simulated dissolution conditions, with a crushed rock sample (1–3 mm) exposed for 30 days to CO_2 supersaturated seawater (0.576 M). Stage-II favoured carbonation conditions; cubic rock specimens (8 cm^3) were brought in contact with the Stage-I seawater sub-saturated in CO_2 (0.095 M).

A multi-analytical methodology was applied to follow the mineralogical and geochemical evolution of rock and seawater during both stages. At the end of Stage-I, the aqueous phase showed a marked increase in iron (Fe), magnesium (Mg) and calcium (Ca) ions and milder increase in silicon (Si) and aluminium (Al) ions. At the end of Stage-II, a decrease in Si and Al concentrations was observed while the Fe, Mg, Ca concentrations still increased, albeit at a lower rate. No significant geochemical variations were detected in the bulk solid phase. The bulk X-ray diffraction (XRD) analyses detected halite as a new mineral phase, while the grazing-XRD design revealed the presence of dolomite. Moreover, the elemental distribution mapping demonstrated the spatial association of carbon with magnesium indicating magnesite crystallisation. The geochemical model developed in CrunchFlow code was able to reproduce the experimental observations and simulate the chemical behaviour for longer time periods.

Overall, the experiments and model point towards a mineral carbonation potential in the Torrão - Odivelas Massif, with further studies being required to upscale the laboratory results to field scale.

1. Introduction

The storage of large volumes of industrial CO_2 in deep geological formations is one of the most promising climate mitigation alternatives, necessary to achieve the goals of the Paris Agreement and the Glasgow Climate Pact to limit anthropogenic warming to 1.5 °C (IEA, 2017; IPCC, 2022). CO_2 storage in geologic reservoirs, such as deep saline aquifers or depleted oil and gas reservoirs, that is, in porous media, has been studied extensively and is a demonstrated technology (GCCSI, 2021).

An alternative geological environment for CO_2 storage is provided by mafic and ultramafic rocks, in which the mineral composition favours the reaction with CO_2 and its precipitation as stable carbonate minerals, such as calcite ($CaCO_3$), dolomite ($CaMg(CO_3)_2$), magnesite ($MgCO_3$) and siderite ($FeCO_3$). This method induces the mineral carbonation of CO_2 and, thereby, allows the permanent sequestration of carbon in a solid phase, eliminating the risk of returning to the atmosphere and

---

* Corresponding author.
E-mail address: e.berrezueta@igme.es (E. Berrezueta).

https://doi.org/10.1016/j.geoen.2023.212010
Received 29 August 2022; Received in revised form 12 June 2023; Accepted 14 June 2023

increasing storage security (Matter et al., 2009; IPCC et al., 2011; IEAGHT, 2011; Sanna et al., 2014). The first step in the mineral trapping process is the dissolution of CO_2 into the brine, which results in carbonic acid. This solution will slowly dissolve silicates, and, under appropriate conditions, divalent cations released by this dissolution can combine with dissolved carbonate ions to form stable carbonates. (Zhang and DePaolo, 2017; Peuble et al., 2017). According to Snæbjörnsdóttir et al. (2020), although *in situ* mineral carbonation, in which CO_2 is injected into a rock massif, offers a large potential volume for carbon storage in formations such as basalts and peridotites (both onshore and offshore), its large-scale implementation remains insufficiently explored beyond laboratory and field-based experiments. Nevertheless, the feasibility of this *in situ* mineral carbonation was demonstrated in two pilot projects; the CarbFix project in Iceland (Druckenmiller and Maroto-Valer, 2005; Gislason and Oelkers, 2014; Matter et al., 2016) and the Wallula project in the USA (McGrail et al., 2014; Wells et al., 2017). The CarbFix project demonstrated that CO_2 dissolution in water during injection reduces the time scale for mineral carbonation to months or few years, discards the need for extensive cap-rocks and allows for shallower injection depths, down to 200 m–300 m (Snæbjörnsdóttir and Gislason, 2016; Stockman, 2012). Still, the vast majority of laboratory and field studies aimed at testing the mineral carbonation in porous volcanic rocks, a geological environment particularly suitable for the technology (Berrezueta et al., 2023). Little work has been done on other mafic and ultramafic lithologies that present similar geochemical composition but more challenging textural and structural conditions. Fractured plutonic mafic and ultramafic rocks may show a reactive behaviour along fractures adequate to enhance the mineral carbonation of small CO_2 sources. Such possibility has seldom been addressed, but given the widespread occurrence of plutonic mafic and ultramafic rock, their potential for mineral carbonation should be investigated, in a first instance through an experimental approach complemented with geochemical modelling.

Experimental studies of mineral dissolution and precipitation rates have been widely used to provide insight into fundamental processes behind mineral carbonation, like predicting the long-term fate of CO_2 stored in basalts and other rocks characterising the relevant gas-fluid-mineral reactions and their kinetics (Zhang and DePaolo, 2017). In an experimental study of Lacinska et al. (2017) on the carbonation of serpentinite and partially serpentinised peridotites, the precipitation was estimated to be approximately 3% wt. In 6.5 months, that is, a hundred times greater than the natural carbonation of Clinton Creek mine tailings in Canada (Wilson et al., 2006) and about 200,000 times greater than the natural carbonation of peridotite in Oman (Kelemen and Matter, 2008). The carbonate precipitation occurred predominantly on the surface of the core and within cross-cutting fractures, an indication that mineral carbonation may be relevant along the fracture planes of plutonic mafic and ultramafic rocks.

Numerical geochemical models have been invaluable tools to study the fate of the CO_2 following injection and to gain insight into the interaction between rock + injected fluids + formation waters (Rogers et al., 2006; Snasbjörnsdóttir et al., 2018). Although there is extensive literature about dissolution rates of individual, common rock-forming minerals when exposed to aqueous solutions of different pH and temperature (e.g., Palandri and Kharaka, 2004), there is ambiguity about how to apply the data to natural-fluid systems (e.g., Steefel, 2008). Among the main limitations of laboratory studies are timescales (experiments usually run for days, weeks or months, rather than years) and spatial scales (e.g., 1 cm^3 to 1 dm^3 sample sizes) (Gysi and Stefánsson, 2012a; Rosenbauer et al., 2005), which constrain the upscaling of experimental results to field scale operation. To solve these limitations, geochemical modelling is used to extend the results over longer time and spatial scales (Gysi and Stefanson, 2012b; Harrison et al., 2019; Moita et al., 2020a). Within the scope of the Portuguese INCARBON project, the selection, classification and characterisation of plutonic ultramafic and mafic rocks was carried out in southern Portugal as potential targets for mineral carbonation, an alternative to conventional CO_2 storage in sedimentary rocks, unavailable in the study region. The industrial area of Sines, in Southern Portugal, is the main CO_2 emission cluster in the country, and since multiple plutonic mafic and ultramafic rock occur in the region, the possibility of implementing mineral carbonation as a CO_2 emissions reduction for the area of Sines is highly relevant for the industrial activity and its emission reduction targets. From a set of ten mapped mafic and ultramafic rock massifs in the study region, a multicriteria decision analysis, including mineralogy, geological structure, surface area, distance to CO_2 sources, expected volume and socioeconomic conditions, led to the selection of the Torrão - Odivelas gabbroic massif as one of the potential targets (Pedro et al., 2020). This article presents the laboratory experiments and geochemical modelling conducted to characterise its potential for mineral carbonation.

The approach used in the laboratory experiments is innovative in its attempts to reproduce the actual physical, thermodynamic and chemical conditions in which mineral carbonation could be implemented in these dense, low porosity, gabbroic rocks. Thus, the experiments use pressure and temperatures conditions similar to ensure supercritical behaviour of CO_2, do not use pure water or additives to enhance mineral carbonation in the laboratory, and instead uses seawater and conducts experiments in two stages to simulate longer interaction periods between rock, seawater and CO_2. The experimental setup is one of the main novelties of this work, and together with the experimental results and its geochemical modelling can provide lead to a new focus on the plutonic for mineral carbonation in mafic and ultramafic rocks.

2. Methodology

2.1. Materials

Pedro et al. (2020) followed a screening and ranking procedure using criteria to identify ultramafic and mafic plutonic rocks with potential for mineral carbonation selected the Torrão - Odivelas Massif (Fig. 1), part of the Beja Igneous Complex (BIC) in Southern Portugal, for detailed laboratory studies.

The BIC is a Variscan magmatic belt with approximately 100 km along the SW boundary of the Ossa-Morena Zone in Portugal. The Torrão - Odivelas Massif has an estimate area of 100 km^2, partially covered by Cenozoic sedimentary formations, and occurs in the western sector of the BIC, inside the Banded Gabbroic Sequence which comprises different succession of gabbroic rocks. Despite the Variscan collisional faults and thrust bordering the BIC, the Torrão – Odivelas Massif displays a N70°E and N15°W subvertical fractures set, without evidence of movement or with a rare strike-slip component, and a third one (N44°W; 25°SW), sometimes parallel to the orientation of the magmatic layering and decompression cracks. The sample used in this study is a gabbro-anorthosite from the Torrão – Odivelas Massif, collected from a small quarry (38°9’38’’; −8°9’22") with a near-horizontal magmatic layering (Fig. 1).

The selected gabbro-anorthosite is a mesocratic rock, with medium to coarse phaneritic texture. It is composed of Ca-plagioclase (70–75 vol %), olivine (20–25 vol%), diopside (5–10 vol%) and Fe–Ti oxides (<5 vol%) (Fig. 2). The plagioclase appears as subhedral elongated crystals and the olivine as anhedral rounded crystals. The diopside occurs around the olivine crystals and reaction textures of thin amphibole fringes can be observed on the borders. The Fe–Ti oxides are inclusions situated inside fractures or bordering the olivine and diopside crystals.

The aqueous phase used in the experiment is seawater (Atlantic) collected on the northern coast of Spain, at the longitude of the city of Gijón. It was kept sealed at a temperature of 291.15 K 18 °C and filtered (0.45 μm) before being used in the experiments. The CO_2 is from a commercial source, supplied at a concentration of 95 vol%.

2.2. Experimental procedure

The laboratory experiments were designed to replicate i) the early

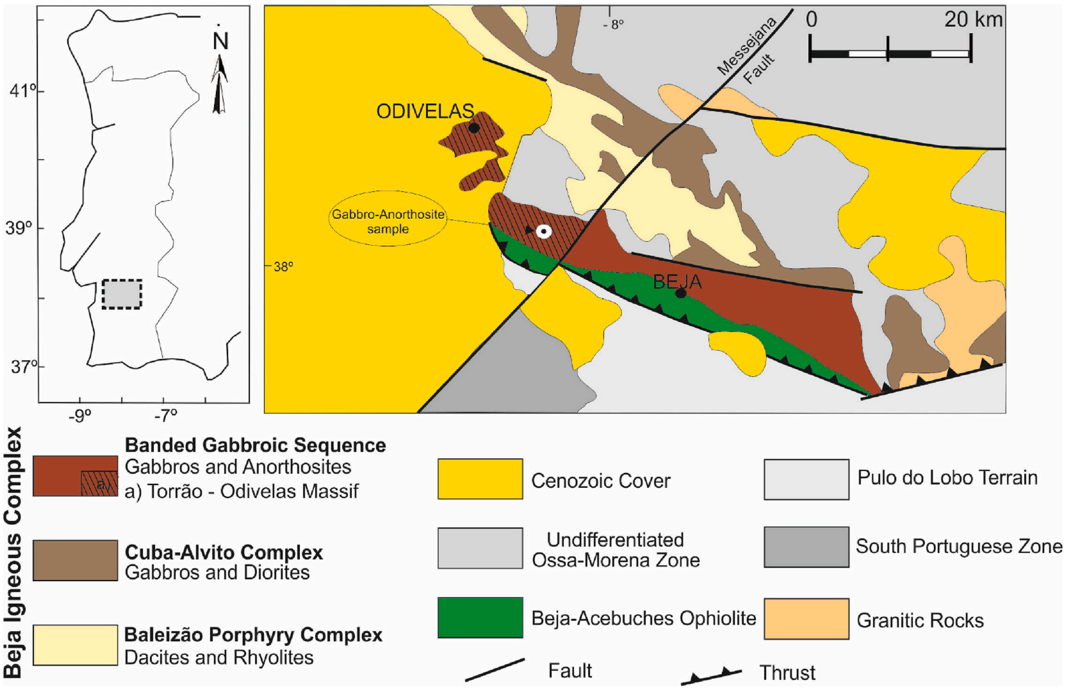

Fig. 1. A simplified geological map of the Beja Igneous Complex (adapted from Jesus et al., 2003 and Pedro et al., 2013).

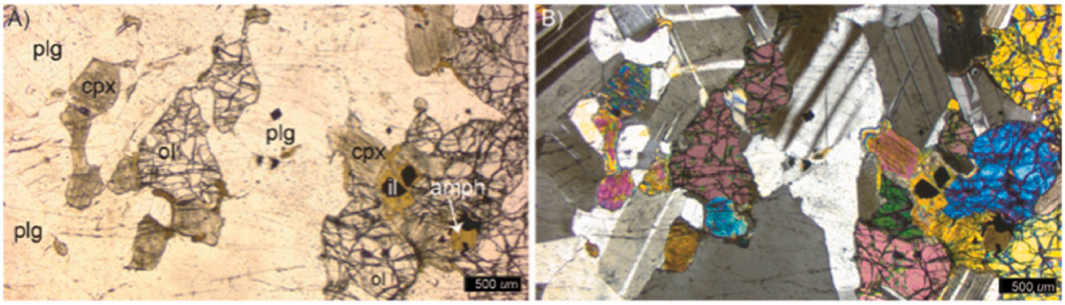

Fig. 2. Microphotograph of the studied gabbro-anorthosite sample from the Torrão – Odivelas Massif, A) Plane polarised light; B) Cross polarised light.

stages of interaction between the mineral phases and a brine supersaturated in CO_2, as expected around an injection well (this is called Stage-I), and ii) the later stages of interaction between the mineral phases and a brine subsaturated in CO_2 and enriched in cations dissolved in earlier stages, as expected in areas farther from the injection well (this is called Stage-II) (Fig. 3A–B) (André et al., 2007). The autoclave used in these experiments is installed in the Tres Cantos Laboratory of the Spanish Geological Survey (Instituto Geológico y Minero de España) (Fig. 3C) and, the followed procedure is based on previous works described by Berrezueta et al. (2016) and Moita et al. (2020b). The autoclave has two CO_2 cylinders (standard industrial CO_2 at 4.5 MPa) that are connected to the other elements of the system by steel connectors (diameter: 5 mm). The first CO_2 cylinder is directly connected to the sample chamber. The second CO_2 cylinder is connected to a piston pump that operates with a flow of 0.01 g/s. In case of gas leakage in the chamber during the experiment, this pump maintains the experimental pressure defined for the test. The inside of the chamber (capacity of 2 dm^3) is coated with polytetrafluoroethylene (PTFE) to protect the material against corrosion. At the bottom of the chamber, a thermostat controls the internal temperature. The calorimeter and pump are connected to the chamber with pressure and temperature sensors and are connected to a computer.

The two experiments consisted of the exposure of a gabbro-anorthosite sample to a CO_2-saturated brine (i.e., CO_2-rich brine) in the autoclave under pressure (P) of 8 MPa and temperature (T) of 313.15 K, without flow. The P and T conditions were selected to exceed the SC CO_2 point and to simulate the conditions of field-scale CO_2 injection and storage. In Stage-I, rock + seawater + CO_2 (~0.576 M) was used, while in Stage-II, rock + seawater + CO_2 (~0.095 M) was used. The ionic strength of solutions were measured using ideal gas equation.

Stage-I (Table 1), with an exposure period of 30 days, aimed to enhance cation availability in the seawater through the dissolution of rock-forming minerals during the early stages of interaction between rock, seawater and CO_2. For this purpose, crushed rock (1–2 mm diameter) was used to increase the specific surface. The resulting enriched seawater was then used (after 3 h and pH increase to ≈7) in Stage-II.

Stage-II (Table 1), with an extended exposure period (90 days), was designed to favour precipitation (i.e. mineral carbonation) using the enriched seawater from Stage-I and cubic rock samples of 8 cm^3. The proportion between rock, seawater and injected CO_2 was different from Stage-I, as the availability of CO_2 was considerably lower. This condition, on the one hand, simulates the decrease in CO_2 concentration as moving away from the injection well and, on the other hand, ensures that pH conditions are more appropriate for mineral carbonation.

Both experimental runs comprised three stages: (a) pressurised CO_2 injection for 3h, starting from 4.5 MPa to 20 °C up to the SC conditions; (b) a pressurised s stabilisation, the actual test period, with no CO_2 flow inside the chamber; and (c) a CO_2 pressure release, from supercritical

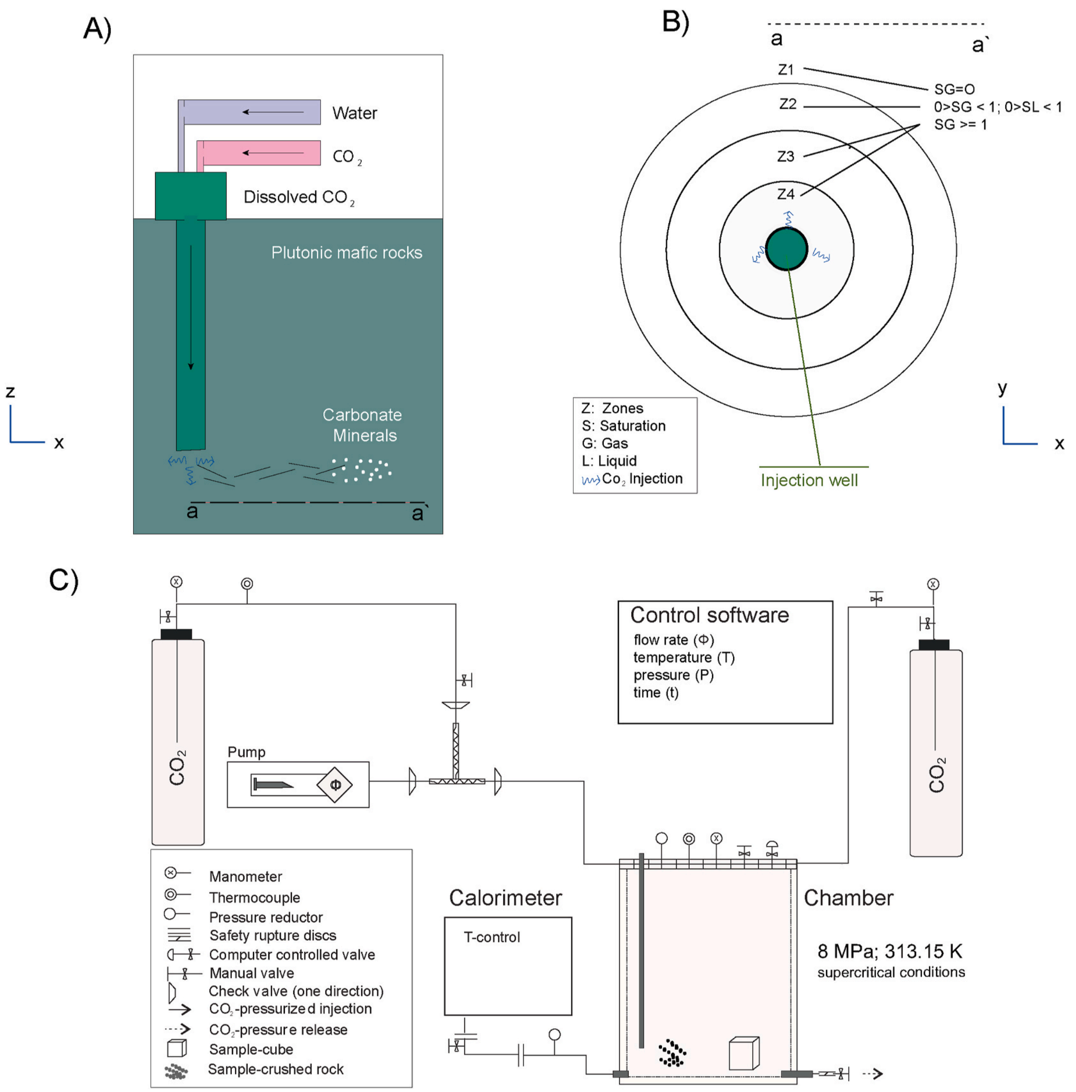

Fig. 3. A) Schematic of CO_2 injection into rocks with simultaneous water injection (Based on the Carbfix method); B) Conceptual diagram of the reactive zones (Z1, Z2, Z3, Z4 and Z5) around the injection well according to André et al. (2007); C) Layout of the experimental setup. Reactor system used for the pressurised CO_2 injection at IGME. Modified from Berrezueta et al. (2016) and Moita et al. (2020b).

Table 1
Experimental conditions (Stage-I and Stage-II) of rock–brine–CO_2 interaction in an autoclave.

-	Sample	Rock (cm^3)	Specimens	Brine (cm^3)	CO_2 (cm^3)	Pressure MPa	Temperature K	Run (Days)
I	Gabbro anorthosite	100	Crushed rock	1550	350	8	313.15	30
II	Gabbro anorthosite	1050	Cubes (8 cm^3)	920	30	8	313.15	90

conditions to ambient conditions, for a similar time period as the pressurisation in stage (a) (i.e. 3h), following the chamber manufacturer recommendations.

2.3. Analytical techniques

The analytical techniques used to identify mineralogical, textural and chemical changes due to SC CO_2 exposure were similar to those applied previously (Moita et al., 2020a, b; Pedro et al., 2020). The analyses were performed at the HERCULES Laboratory (University of Évora, Portugal).

i) Thin-section petrography was performed with a Leica bright-field optical microscope (LEICA DM 2500P, Wetzlar, Germany);
ii) X-ray powder and *in situ* diffractograms were produced using a Bruker AXS-D8 Discover (Bruker Corp., Billerica, MA, USA), with Cu-Kα radiation ($\lambda = 0.1540598$ nm), under the following conditions: scanning between 3° and 75° (2θ), scanning velocity of 0.05° 2θ/s, accelerating voltage of 40 kV, and current of 40 mA. To evaluate the mineralogical composition of the specimen surface, *in situ* grazing incidence geometry experiments were conducted, with an incidence of 1.5° and 2θ scanning from 8 to 60°;
iii) Surface chemical analysis was performed using Scanning Electron Microscopy with Energy Dispersive Spectroscopy (SEM-EDS), using a Hitachi S–3700N SEM (Hitachi High Technologies, Berlin, Germany), coupled with a Bruker XFlash 5010 SDD detector (Bruker Corp, Billerica, MA, USA). The analysis was performed under a low vacuum of 40 Pa, with a current of 20 kV. A Bruker

Hyperion 3000 infrared spectrometer was used, equipped with a single-point MCT detector cooled with liquid nitrogen and a 20× ATR objective with a Ge crystal of 80 μm diameter;

iv) X-ray fluorescence (XRF) was applied for whole-rock geochemical analysis, concretely for the quantification of major oxides (SiO_2, TiO_2, Al_2O_3, Na_2O, K_2O, CaO, MgO, MnO, FeO, P_2O_5), sulphur and some minor elements (Rb, Sr, Y, Zr, Nb, Ba, Cr, Co, Ni, Cu, Zn). Analyses were performed with an S2 Puma energy-dispersive X-ray spectrometer (Bruker), using a methodology similar to that adopted by Georgiou et al., (2015). A description of the standard reference materials (SRM) utilised in the calibration method can be found elsewhere (Beltrame et al., 2019). After the determination of loss on ignition (LOI), samples were fused in a Claisse LeNeo heating chamber, using a flux (Li−tetraborate) to prepare fused beads (ratio sample/flux = 1/10). The software utilised for data acquisition and processing was Spectra Elements 2.0, which reported the final oxide/element concentrations and the instrumental statistical error (Stat. error) associated with the measurement.

The brine analyses (Na^+; K^+, Mg^{2+}, Ca^{2+}, SO_4^{2-}, Cl^-, HCO_3^-, SiO_2) were performed at the Spanish Geological Survey (IGME, Madrid, Spain) by ion chromatography (Dionex 600 de Vertex) and ICP-OES (Varian Vista MPX) before and after each experiment. In addition, both in Stage-I and Stage-II, the Fe and Al content of the brine was determined at the HERCULES Laboratory (Évora, Portugal) with an Agilent 8800 ICP Triple Quad (ICP-QQQ), operating with an RF power of 1550 W, RF matching of 1.7 V, a sample depth of 10 mm, carrier gas (Ar) of 1.1 L/min and plasma gas (Ar) of 15 L/min. Prior to the analysis, the equipment was calibrated with a tuning solution from Agilent, the sensitivity and resolution were optimised and the doubly charged ions (<1.84%) and oxides (<1.10%) were minimised.

2.4. Geochemical modelling

2.4.1. Modelling tool

Simulations were performed using CrunchFlow (Steefel and Lasaga, 1994; Steefel, 2009), a multicomponent reactive-transport code for studying fluid-rock interactions in porous media. This reactive transport code has many advantages, such as a complete equilibrium thermodynamic treatment, flexible kinetic rate law formulations for each mineral depending on the reaction mechanism, and a range of 3D flow capabilities. The mineral dissolution in aqueous phases and the precipitation of secondary phases are kinetically controlled, thus a reaction rate is given in terms of primary species. The reaction kinetics are treated based on the transition state theory (TST) (Steefel and Lasaga, 1994; Steefel, 2009; Steefel et al., 2014).

In the present study, the reaction rate was described only as a function of time. All parameters controlling the kinetic reaction rate (initial brine concentration, aqueous CO_2 concentration, mineral composition, and reactive surface) were evaluated. The Crunchflow simulator considers the transition state theory (TST) to define the reaction rate, which is directly dependent on the saturation state of minerals (derived from experiments and confirmed by speciation simulation), the kinetic constant (derived from literature, Palandri and Kharaka, 2004; Xu et al., 2005) and the reactive surface (Xu et al., 2004). A poor evaluation of the reactive surface area (RSA) will contribute to significant uncertainties in the quantitative simulation of chemical processes. Currently, there is no universally accepted method for estimating average mineral reactive surface areas. Usually, a range of approximations is adopted based on easily measurable attributes. These approximations to the reactive surface area are then calibrated on mineral dissolution rates by comparison between modelling and experimental results.

2.4.2. Input conditions for rock and fluid

The experimental results were numerically reproduced based on two different reactive surface definition approaches. In Stage-I, where the crushed rock was reacted, the dissolution rate was calculated using the mineral grain size geometry approach for reactive surface (Bekhingham et al., 2016; Abdoulghafour et al., 2021). Abdoulghafour et al. (2021) applied the spherical geometry approach with satisfactory results, making it possible to change the mineral fraction volume during the simulation.

In Stage-II, where the samples are cube-shaped, the reactive surface area was estimated using the fractal approach (Sonnenthal and Spycher, 2001). The cubes were arranged inside the autoclave to allow the CO_2-rich brine to be in contact with the cube surfaces, triggering surface mineral dissolution/precipitation reaction, similar to those expected at a large scale due to percolation of CO_2-rich brine along the fracture networks.

The surface geometry of the crushed rock (GSA) and the surface geometry of cube-shaped samples (A_r) can be respectively assessed as described in Equations (1) and (2):

$$\mathrm{GSA} = \frac{\mathrm{A_s}}{\mathrm{V}} \tag{1}$$

where *As* is the grain surface, which is a function of the average grain diameter (0.15 mm), and *V* is the crushed rock bulk volume;

$$A_r = \frac{A_{f-m}}{2\varphi_{f-m}} \tag{2}$$

$$A_r = \frac{A_{f-m}}{2\varphi_{f-m}}$$

$A_{f\text{-}m}$ is the cube-matrix total area to volume ratio and φ_{f-m} is the fracture porosity of the rock.

The $A_{f\text{-}m}$ value, in Equation (3), is determined considering the cube surface (S_c) to volume (V_c) ratio and the crushed rock surface (Ss) to volume (V_s) ratio and multiplied with the mineral volume fraction (f_m). *N* represents the number of cubes in the autoclave.

$$A_{f-m} = f_m\left(n\frac{S_c}{V_c} + \frac{S_s}{V_s}\right) \tag{3}$$

The fracture porosity, in Equation (4), is the ratio between the fracture volume (V_f), which is the void between adjacent cube surfaces, and the bulk volume (V_t).

$$\varphi_{f-m} = \frac{V_f}{V_t} = \frac{n \bullet e \bullet a^2}{V_t} \tag{4}$$

a is the cube edge length and *e* the spacing between opposite surfaces.

In Stage-I, the area to volume ratio of the sand-size crushed rock was 660 m^2/m^3. Considering an average porosity of sand of $\varphi = 0.34$ (Hudak, 1994), the reactive surface of all the crushed rock is 1470.7 m^2/m^3. The reactive surface of each mineral phase was determined considering the molecular weight over the mineral density times the volume fraction (Equation (5)).

$$A_{bulk} = \varphi_m \bullet GSA \bullet M_w / \rho_m \tag{5}$$

The resulting reactive surfaces are reported in Table 2. The sand volume (100 cm^3) represents only 6% of the volume (brine + rock); thus, each mineral surface was multiplied by this fraction after the adjustment with the mineral parameters (Equation (5)).

In Stage-II, the total volume occupied by the rock was 1050 cm^3 and the total surface of cubes was estimated to be 3072 cm^2; therefore, the area to volume ratio was 2.92 cm^2/cm^3. The total fracture volume was estimated to be 76 cm^3 yielding a total fracture porosity of 0.073. The resulting reactive surface was therefore 2007.8 m^2/m^3. To determine the reactive area of each mineral, the total area was multiplied by the

Table 2
Reactive surface of the studied minerals in the crushed rock sample (sand) and in the cubes.

Minerals	Volume fraction (%)	Reactive surface (m^2/m^3): sand	Reactive surface (m^2/m^3): cubes
Albite	0.08	24.04	67.44
Anorthite	0.68	187	863
K feldspar	0.012	5.88	56.2
Diopside	0.047	12.93	36.14
Forsterite	0.067	30.92	41.36
Fayalite	0.042	46.97	40.15
Enstatite	0.01	14	28.11
Ferrosilite	0.01	12	22.05

volume fraction of each mineral (Table 2).

According to the mineralogy of the dominant gabbro-anorthosite end-member mineral phases (Table 2), i.e., plagioclase (anorthite-albite), pyroxene (diopside, enstatite, ferrosilite) and olivine (forsterite and fayalite), the cations with the highest concentration in the rock are calcium, magnesium and iron.

The initial seawater composition is shown in Table 3 (0-days composition); reactants in Stage-I and the fluid chemistry after 30 days were used as the input composition for the simulation in Stage-II (Table 3).

3. Results

3.1. Mineralogical and chemical evolution of the rocks

The mineralogical composition of the tested gabbro-anorthosite defined by the bulk XRD analysis (Table 4) agrees with the above petrographic analysis. The used samples were not weathered, as revealed by the low Loss on Ignition (LOI) value. The chemical composition (Table 5), specifically the concentration of SiO_2 (49 wt%) and MgO (7.5 wt%), is consistent with the basic nature of the rock.

There were no noticeable differences in the bulk chemical composition throughout the experiment (i.e. 0-day, 30-day and 90-day tests). Variations in terms of major and minor elements were not significant. The only significant difference was the Cr and Ni-enrichment at 30 days, possibly related to a higher amount of chromite in the powdered fraction.

Regarding the mineralogy of the solid phase, halite was detected both after Stage- I and Stage-II. In bulk XRD analysis, any small amounts of newly formed phases will be masked by the volumetrically more abundant phases.

Since the rock specimen did not have consequential primary porosity, the presence of new phases was expected to occur on the surface of the specimens and not as interstitial phases. Thus, the surface of the specimens was analysed by grazing XRD (Fig. 4). This method is a discrete analysis that scans areas on the surface of the sample. The diffractogram in Fig. 4 shows a peak at $2\theta = 31^\circ$ that indicates the presence of dolomite, a carbonate not detected in the specimens before the carbonation experiment, alongside diopside, halite, and plagioclase. Since it is not representative of the volume, the height of peaks should not be considered for quantification.

Table 3
Chemical composition of the solution used as input in the simulation.

Components	Input for Stage-I (0 days) ($molkgw^{-1}$)	Input for Stage-II (30 days) ($molkgw^{-1}$)
Ca^{2+}	0.0112	0.0135
Mg^{2+}	0.0576	0.065
Na^+	0.648	0.79
K^+	0.0141	0.0144
SO_4^{2-}	0.0291	0.031
Cl^-	0.726	0.845
HCO_3^-	1.09	1.09
SiO_2	3.3×10^{-6}	0.00128
Fe^{2+}	9.4×10^{-6}	0.0012
Al^{3+}	4.7×10^{-6}	0.00073
pH	8.10	4.75

Texturally comparing the specimens before and after the 90 days of Stage-II, no dissolution was observed as in a similar previous experiment (Moita et al., 2021a). With less magnification, it is clear that the enrichment in Cl and Ca (Fig. 5) occurs due to the precipitation of halite that occurs during the drying in the oven (313.15 K), after the experiment.

At a higher magnification, the elemental chemical distribution obtained by SEM-EDS showed occasional spatial association of carbon with Mg (Fig. 6). This association is clearly not related to silicate minerals since silicon and aluminium have a different spatial distribution.

3.2. Chemical evolution of the seawater

The fluid (i.e., the seawater) used in the experiments (Stage-I and Stage-II) was recovered immediately after the end of the runs, for chemical analysis (at 30 days and 90 days, respectively, Table 6). The brine collected after 30 days was used as the initial fluid for the Stage-II experiments.

In Stage-I, elements concentrations generally increased: Na^+ (21 wt %), Ca^{2+} (20 wt%); K^+ (2 wt%), Mg^{2+} (13 wt%), total Fe (12,658 wt%), SiO_2(37,940 wt%) and Al (1492 wt%).

The anions SO_4^{2-} and Cl^-, not present in the solid rock, maintained their original concentrations after 30 days. The initial seawater pH of 8.1 dropped to 6.1 after the CO_2-seawater-rock interaction (measured just after concluding the test) (Table 6).

In Stage-II, the behaviour of cations in solution was variable: the concentration of Ca^{2+} (26 wt%), Mg^{2+} (3 wt%) and total Fe (33 wt%) increased, while that of Na^+ (3 wt%) and K^+ (14 wt%) decreased. In addition, SiO_2 (66 wt%) and Al (72 wt%) decreased, and SO_4^{2-} and Cl^- did not show variation. The initial pH of 7.0 (measured just before beginning the test) dropped to 6.32 (measured just after concluding the test) after CO_2-seawater-rock interaction (Table 6).

3.3. Modelling results

3.3.1. Fluid chemistry and secondary minerals

The simulation results in **Stage-I** were presented in terms of the evolution of fluid pH, the concentration of dissolved CO_2 and the concentration of dissolved major cations. For the 30 days simulation, the fluid (seawater with CO_2) remained acidic, and pH increased slightly from 4.60 to 4.73 (Fig. 7A). Simultaneously, the dissolved CO_2 concentration, CO_2 (aq), remained constant during the simulation time, indicating that only dissolution occurred (Fig. 7A). Therefore, the increase in pH and the constant CO_2(aq) imply a dissolution dominant stage for the primary minerals. The dissolution process correlates with the increase in calcium and magnesium concentration from the initial seawater concentration to 540 $mg.L^{-1}$ (a variation of 17%) and 1502 $mg.L^{-1}$ (a variation of 7 wt%), respectively (Fig. 7B). Experimental calcium and magnesium concentrations confirmed these results (Table 5).

The concentration of iron (originally under the detection limit) increased suddenly on day-1 before decreasing sharply (Fig. 8). Simultaneously, aqueous silica also increased strongly from the initial low concentration (10 $mg.L^{-1}$) to 300 $mg.L^{-1}$ in the first 2 days, before decreasing to a value around 200 $mg.L^{-1}$ at t = 30 days (Fig. 8). The measured Fe^{2+} (67.62 $mg.L^{-1}$: experimental measure) is in the order of the simulation (30.2 $mg.L^{-1}$), the measured SiO_2 (76.8 $mg.L^{-1}$: experimental measure) is three times lower than the simulated value (228 $mg.L^{-1}$, respectively) but still within the same order of magnitude.

The Stage-II simulation used the reactive surface area estimated by the fracture geometric approach (Table 2) and the brine properties from Stage-I. The simulated pH increased (Fig. 9A) from the initial value of

Table 4
Mineralogical composition determined by bulk XRD on powdered samples (++++ very abundant; ++ abundant; +present; tr. Trace amount).

Sample	Diopside	Amphibole	Plagioclase	Clino-pyroxene	Vermiculite	Talc	Lizardite	Forsterite	Halite
ODF_1A (powder)	++	+	++++	+	tr	tr	+	+	
ODF 1A 30 days (sand)	++	++	++++			++	++	++	++
ODF 1A 90 days (specimens)	++	++	++++			tr	+	+	+
ODF 1A (white sand)	++	++	++++			+	+	+	+

Table 5
Whole-rock geochemistry of the gabbro-anorthosite by XRF.

Components	ODF_1A (powder)	ODF_1A (with sand)	ODF_1A 30 days (sand)	ODF_1A 90 days (specimens)
Major elements (wt.%)				
SiO_2	49.87	49.18	49.71	48.50
TiO_2	0.24	0.25	0.24	0.25
Al_2O_3	21.55	21.27	21.48	21.24
Na_2O	3.21	3.09	2.99	2.81
MgO	7.83	7.50	7.64	7.40
Fe_2O_3	5.91	5.98	5.92	6.09
MnO	0.11	0.10	0.11	0.10
K_2O	0.07	0.06	0.01	0.07
CaO	11.24	10.88	11.04	10.64
$P2O_5$	0.08	0.08	0.08	0.08
LOI	0.87	2.63	2.74	3.62
Trace elements (ppm)				
Rb	7.67	5.60	6.49	4.79
Sr	538.72	517.51	523.50	526.48
Y	10.63	9.86	8.10	8.87
Zr	31.68	28.79	30.00	30.29
Nb	28.27	31.71	32.29	29.18
Ba	973.39	1025.66	1013.07	868.31
Cr	682.27	227.9	1008.38	260.61
Co	45.72	43.59	40.86	59.72
Ni	317.38	135.51	624.38	131.86
Cu	63.92	67.15	63.59	99.42
Zn	30.13	29.35	26.20	21.74

4.75–5.70, while the CO_2 (aq) concentration decreased slightly from 0.09 mol.L^{-1} to 0.06 mol.L^{-1} at 90 days, corresponding to a decrease of 27 mol.%, and decreased further to values below 0.05 mol.L^{-1}, after 120 days. The continuous decrease observed from pH = 5.30, after the 20 days, testified the consumption of CO_2 over time.

Calcium and magnesium concentrations increased during the simulation time, as shown in Fig. 9B, and this was also confirmed by the experimental results. Again, the simulation results reproduced the experiment because the uncertainty between the experiment and simulated concentration is < 20 wt% for calcium and 6 wt% for magnesium. As the rock contains more than 80 wt% of Ca-plagioclase, the continued dissolution of Ca^{2+} beyond 90-days can be explained by its abundance in the initial rock.

The simulated iron and silica evolution matched the experimental data with non-negligible differences. At 90 days, the measured experimental silica and iron concentration values were 30 mg.L^{-1} and 95 mg.L^{-1}, respectively, compared to the 3.8 mg.L^{-1} and 189 mg.L^{-1} values obtained by modelling (Fig. 10). However, iron and SiO_2 were measured using different methods than calcium and magnesium.

3.3.2. *Mineral evolution*

During Stage-I, the fraction volume of olivine (forsterite-fayalite; Fig. 11A), plagioclase (anorthite) and pyroxene (diopside; Fig. 11B) decreased by 1–2 units without the formation of a significant amount of secondary minerals.

During Stage-II, secondary minerals, including silicates and carbonates, were predicted to precipitate (e.g., dolomite around 80 days); a very small amount of carbonates (0.02 vol% of siderite and 0.006 vol% of dolomite) were estimated (Fig. 12).

4. Discussion

Previous laboratory experiments on mineral carbonation have invariably recorded very small amounts of carbonates precipitation, mostly due to the short time periods for which the experiments can be run, but also reflecting the small size of the rock samples that render the observation of the newly formed carbonates very difficult. To stimulate the precipitation of carbonates, experimental works have often resorted to additives to control the pH conditions and the use of crushed rock to increase the reactive surface area. That was not the approach used in this study, which privileged reproducing realistic field conditions. This section discusses the results obtained by reconciling observed and simulated result to understand the chemical processes acting in the fluid

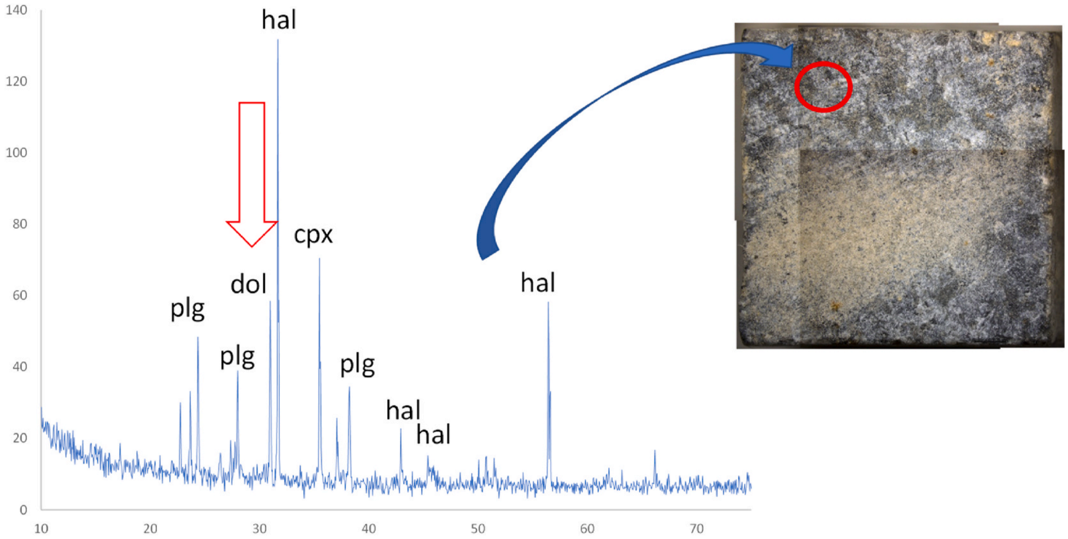

Fig. 4. Grazing diffractogram obtained on the surface of the sample; plg – plagioclase, hal – halite, cpx – clinopyroxene, dol-dolomite.

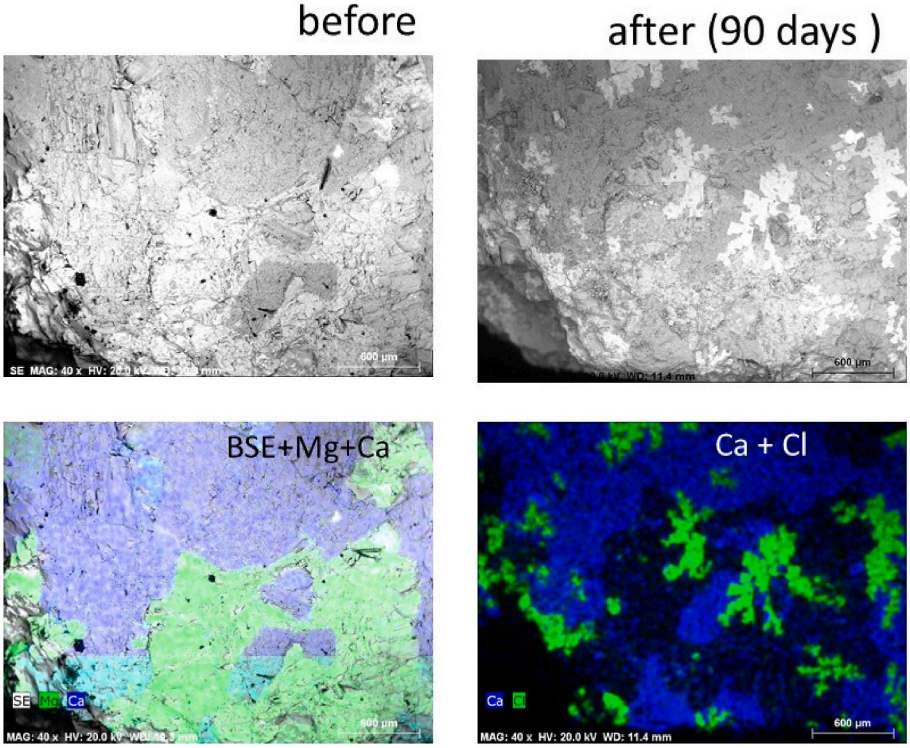

Fig. 5. SEM-EDS images of a gabbro-anorthosite specimen before (left) and after (right) interaction with SC CO_2-rich brine, during Stage-II.

and mineral phases, and by discussing the adequacy of the experimental setup for reproducing field conditions that might be encountered in a field experiments for mineral carbonation in the targeted mafic rock.

4.1. Geochemical variations (brine)

The Ca^{2+}, Mg^{2+} and total Fe concentrations increase in the seawater observed during Stage-I (20 wt%, 13 wt% and 12,658 wt%, respectively) and in Stage-II (25 wt%, 2 wt% and 33 wt%, respectively). This increase was expected in Stage-I, during which dissolution of magmatic mineral phases prevailed due to the acidic brine and the dissolution was enhanced by the high specific surface of the crushed rock. In fact, as projected by the geochemical model, the initial seawater charged with 1.09 mol/L of CO_2 was prone to dissolve Ca-plagioclase (delivering Ca^{2+}, SiO_4^{2-} and Al^{3+}), olivine (the most reactive mafic phase, delivering Mg^{2+}, Fe^{3+} and silica) and, in less extent, diopside (delivering Ca^{2+}, Fe, Mg^{2+}, Si^{4+} and Al^{3+}). Despite the significant difference observed in the measured and simulated pH, the Ca^{2+} and Mg^{2+} experimental concentrations were correctly reproduced by the simulation. Consequently, we assume that the actual pH in the reactor after 30 days ranged from 4.7 to 5.0 as indicated in the literature for such thermochemical conditions, and as suggested by other experimental works carried out in autoclave (e.g., Gysi and Stefanson, 2012a, b; Luquot and Gouze, 2009; Tarkowski et al., 2014). Modelled iron and silica concentrations were in the range of the experiment (within the same order of magnitude). The difference between the experiments and simulation data is related to the stoichiometric dissolution in the simulation versus the incongruent dissolution in the experiment.

Modelling of Stage-II predicted a pH increase from an initial pH charge equivalent to 4.75 (similar to Stage-I), to pH = 5.60 after 90 days of simulation, which is compatible with the experimental results showing that, during Stage-II, mineral dissolution was still taking place due to the still acidic pH, although it was less intense than in Stage-I. Silica and aluminium concentrations increase at 30-day runtime (37,940 wt% and 1494 wt%, respectively) reflect this behaviour. For longer time periods, the geochemical model explains the observed, decrease in Silica and Aluminium (66 wt% and 72 wt%, respectively) at 90 days by their consumption by precipitation as new solid phases. In fact, the model shows that, CO_2 concentration started to decline slightly after 20 days of simulation. This CO_2 decrease is associated with a moderate increase in the cation concentrations, mainly calcium and magnesium, in agreement with the results of the experiment.

In general, the variability of the concentration of elements in the seawater (Table 6: Stage-I and Stage-II) reflects the reaction dynamics imposed by the rock composition (Table 5), the experimental conditions (Table 1) and the composition of the seawater.

4.2. Mineralogical variations

The experimental mineralogical results obtained after 30 (Stage-I) and 90 (Stage-II) days are generally in agreement with the modelled prediction. That is, the association of carbon and magnesium detected on the surface of the specimens, after 90 days, concurs with the predicted magnesite ($MgCO_3$) formation. Additionally, the dolomite encountered by the grazing XRD diffractogram reflects the contribution of magnesium in the carbonation process.

The phyllosilicates and zeolites, predicted by the modelling, are not detected by any of the used analytical techniques. Nevertheless, the decrease in silica and aluminium oxide associated with similar behaviour for Na and K in the brine can be explained by the modelled precipitation of kaolinite and mesolite. According to the modelled results, kaolinite and mesolite, associated with small amounts of siderite, are the first secondary phases to precipitate, followed by dolomite formation beyond the observation period. The decrease in dissolved CO_2 (20 vol% with respect to the initial concentration), predicted by modelling for times shorter than 90 days could be associated to the early formation of a small amount of siderite ($<1 \times 10^{-4}$ vol%). The sharp breakthrough of the iron and silica concentration in the seawater is in agreement with the precipitation of Fe- and SiO_2-rich secondary phases favoured by the pH conditions (pH $>$ 5.0 at t $>$ 20 days). Furthermore, up to 90 days and more, the amount of carbonates and other secondary phases, including clays, increased to 0.32 vol%.

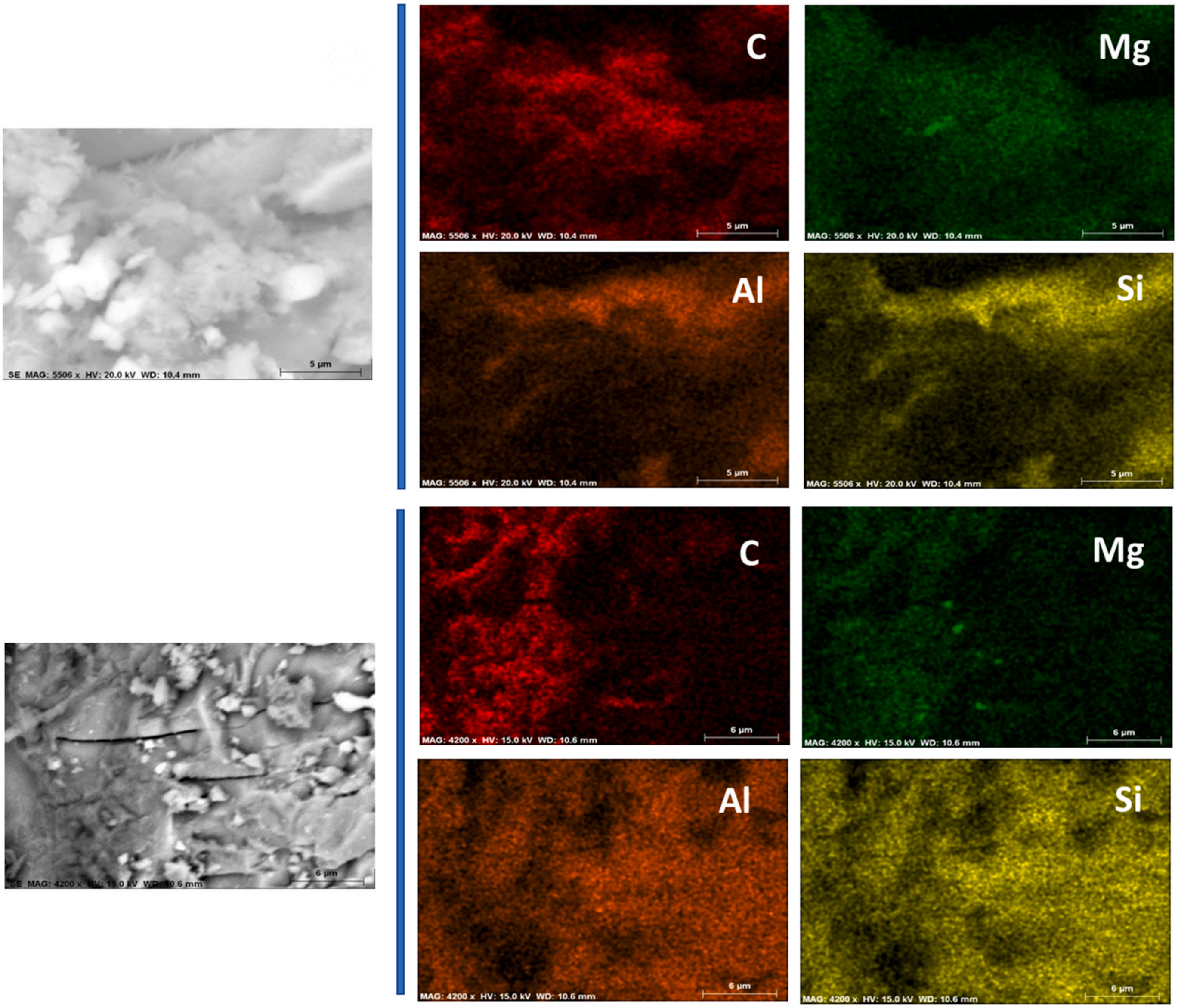

Fig. 6. SEM-EDS images of a gabbro-anorthosite after Stage-II (90days) for two areas A and B. Backscattered electron image (BSE) and respective elemental distribution for carbon (C), magnesium (Mg), silicon (Si) and aluminium (Al).

Table 6
Seawater composition at 0, 30 and 90 days. (*at the end of 30 days experiment, ** before starting the 90 days experiment).

Elements	Brine 0 days	Brine 30 days	Brine 90 days
	(mg/L)	(mg/L)	(mg/L)
Na^+	14,915 ± 2088	18,160 ± 2542	17,600 ± 2464
K^+	552 ± 66	565 ± 67	485 ± 58.2
Mg^{2+}	1400 ± 140	1580 ± 158	1620 ± 162
Ca^{2+}	450 ± 45	540 ± 54	680 ± 68
SO_4^{2-}	2800 ± 392	3000 ± 420	3080 ± 431
Cl^-	25,800 ± 3096	30,000 ± 3600	30,000 ± 3600
HCO_3^-	10 ± 1	10 ± 1	10 ± 1
SiO_2	0.2 ± 0.1	76.8 ± 7.7	30 ± 3
Fe	0.53 ± 0.03	67.62 ± 3.38	94.04 ± 4.70
Al^{3+}	1.26 ± 0.06	20.06 ± 1.00	5.57 ± 0.28
pH	8.10 ± 0.16	6.10* ± 0.12/7.00** ± 0.14	6.32 ± 0.12

The newly formed phases, namely carbonates, are indistinguishable in bulk analyses. The difficulty in detecting new mineral phases comes from their minimal quantity. The observation scale of the images (magnifications of 5000x), in which magnesite crystals of 12 µm size were detected, reveals the difficulty of this approach.

Although there are no significant variations in the global mineralogical and chemical composition of samples from the two experiments, the observed changes could be due to local precipitations/dissolutions at the specimen surface and could represent the early effects of the influence of the CO_2-rich brine on the rock.

4.3. *Conceptual model - approaching real conditions*

The experimental design aimed to reproduce two scenarios that are expected to occur during real CO_2 injection in mafic rocks at around 800 m depth, while adopting the general injection strategy of the Carbfix project as described by Snæbjörnsdóttir and Gislason (2016) and Stockman (2012), in which CO_2 is injected simultaneously with water, promoting CO_2 dissolution within the injection. This procedure ensures that the dissolved CO_2 is immediately available for mineral carbonation as soon as it is in contact with the reactive minerals and prevents the risk of the CO_2 ascending to the surface by buoyancy, since the water with the dissolved CO_2 is denser than the surrounding formation water. A

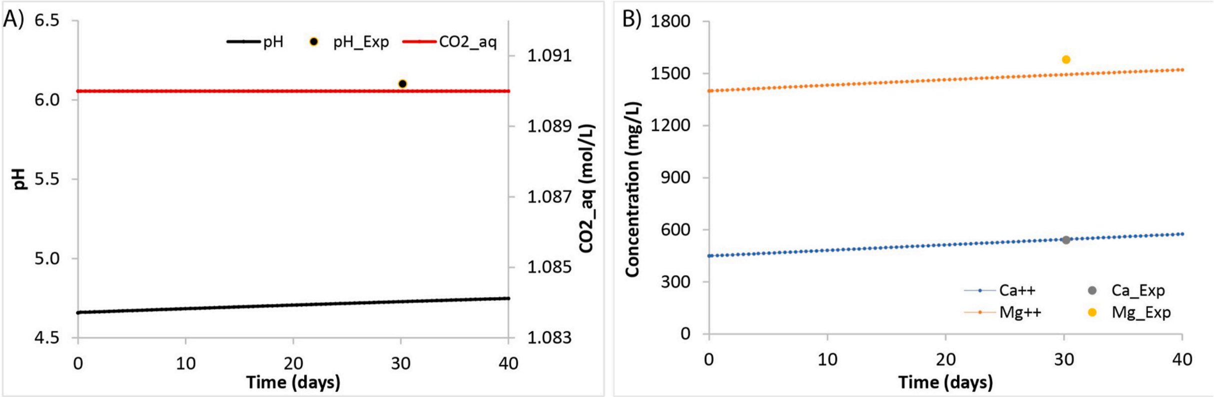

Fig. 7. The evolution of pH and Ca–Mg and their comparison with experimental data during the 30 days run. A) evolution of pH and dissolved CO_2concentration; B) evolution of Ca and Mg over time.

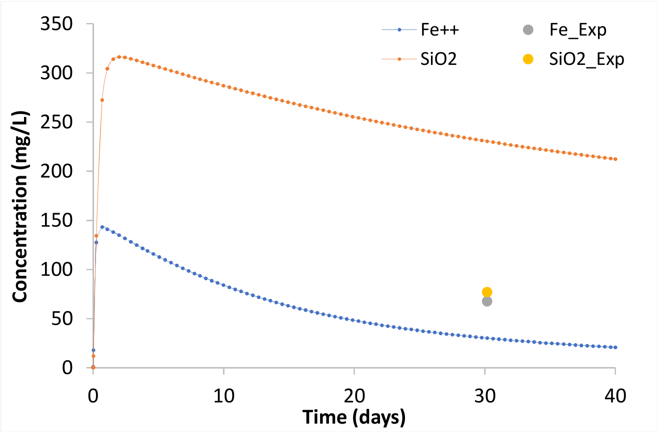

Fig. 8. The evolution of Fe^{2+} and SiO_2 concentration in the solution compared to the experimental data in Stage I.

further consequence of this injection strategy, is the less stringent requirements for reservoir selection, since the presence of a caprock is not essential (Snæbjörnsdóttir and Gislason, 2016; Stockman, 2012).

Stage-I of the described laboratory experiment aims to mimick the conditions of this, early injection phase, with the CO_2 dissolved in seawater and placed in contact with the specimens reproducing chemical reactions favouring mineral dissolution in the immediate vicinity of an hypothecal injection well (Fig. 13A).

Stage-II aims to replicate the conditions expected to take place further from the injection well. "Aging" the brine, i.e. enrichening it in cations and depleting it in CO_2, reproduces the evolution of the fluid along distance from an injection point and the time elapsed since the injection, favouring carbonation. Stage-II can also be envisaged as if the injection is stopped (Fig. 13B); pressure will decrease near the injection point, leaving the enriched brine in non-saturated CO_2 conditions. In this case, carbonation is expected to occur also near the injection point.

Although seawater has been used as brine in other experiments (e.g. Rigopoulos et al., 2018; Wolff-Boenisch and Galeczka, 2018) some authors (Marieni and Oelkers, 2018) mention difficulties in predicting its performance; namely, due to sulphate scaling, clay precipitation and

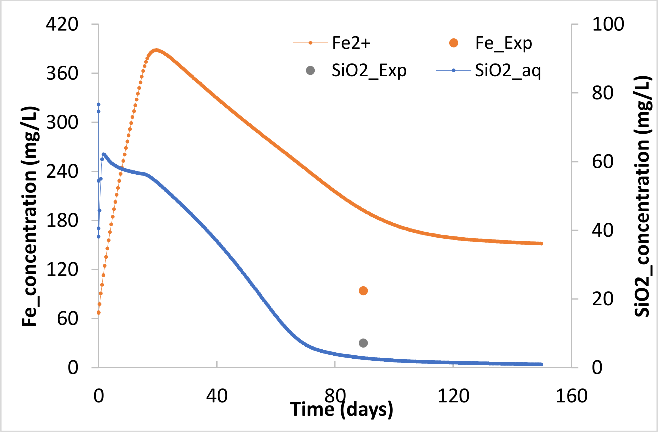

Fig. 10. The evolution of aqueous silica and iron concentration in the solution compared to the experimental data, in Stage-II.

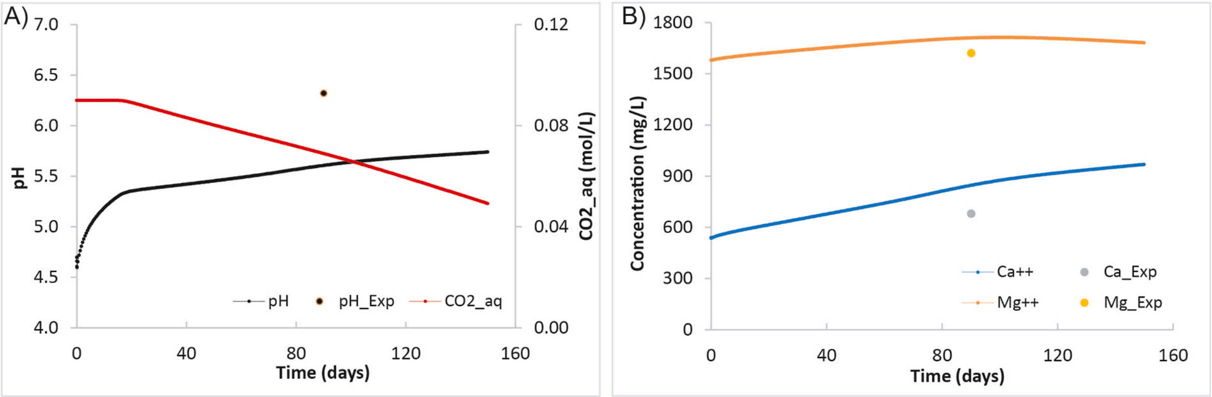

Fig. 9. The evolution of the solution composition over time compared to the experimental data. A) pH and aqueous CO_2. B) Ca^{2+} and Mg^{2+} concentration.

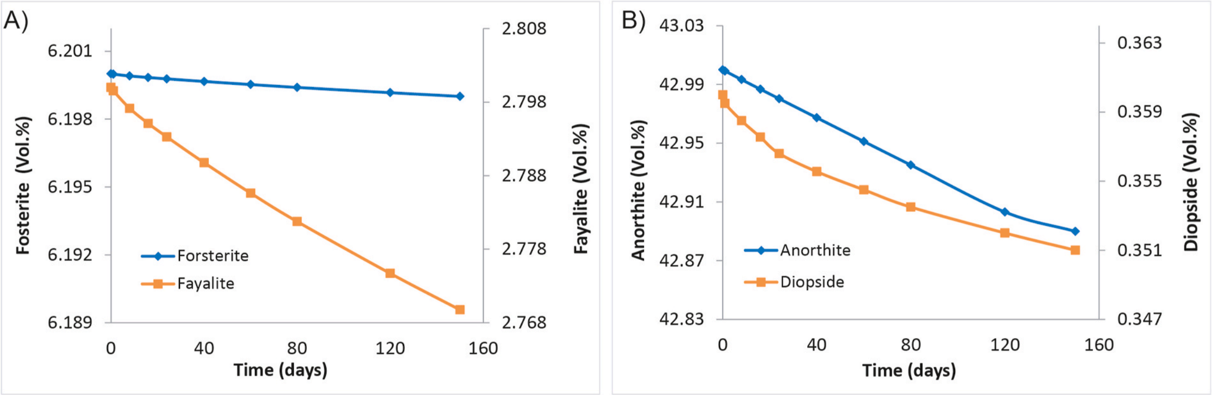

Fig. 11. The evolution (Stage-I) of the simulated volume fraction of the primary minerals (in m^3 mineral/m^3 rock). A) olivine minerals and B) anorthite and diopside.

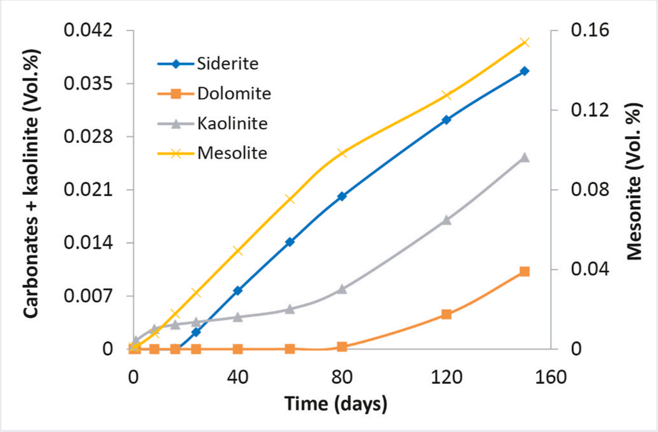

Fig. 12. The evolution (Stage-II) of the simulated volume fraction of the secondary minerals (in m^3 mineral/m^3 rock), due to the dissolution-precipitation mechanisms and the variation of mineral volume fraction.

clogging. These are associated to the lack of information on core scale experiments or optimisation of pH for maximum mineral carbonation. Seawater was used in this work due to its availability and the possibility of using it in larger-scale processes, thus offering an economic advantage when compared to other water sources. Moreover, we did not want to catalyse or manipulate the process by introducing additives (e.g., by controlling acidity with sodium hydrogen carbonate ($NaHCO_3$)) in order to maintain a realistic design of anand economically viable injection. We chose to induce pH variation by changing the CO_2 concentration from Stage-I to Stage-II. This approach and the use of seawater instead of a high salinity brine, resulted in mineral carbonation that had not been obtained in a previous experimental study (Moita et al., 2020b) and allows for a cautious optimism regarding the mineral carbonation of CO_2 in plutonic mafic rocks.

The results obtained demonstrate that mineral carbonation can occur in plutonic mafic rock under conditions similar to those expected for field experiments. However, significant challenges need to be studied to understand what the scale of that mineral carbonation might be. The dense nature of these rocks, with negligible primary porosity, in which flow occurs only along fractures imply that the available reactive surface of the minerals is small, restricted to area of the reactive minerals along the surface planes. Typically, the secondary porosity provided by fractures in this type of rock massif will be in the order of a 1%–2%, with fractures tending for closure with increasing depth. Upscaling of the geochemical model to the massif conditions is currently being conducted to understand the carbonation rates that might be achieved under such conditions. The possibility of increasing the reactive surface area and the injectivity by inducing hydraulic fracturing (e.g., Kelemen and Matter, 2008) is also being investigated.

In any case, the strong reactions that were observed in the Stage-I experiment, in which the reactive surface area was drastically

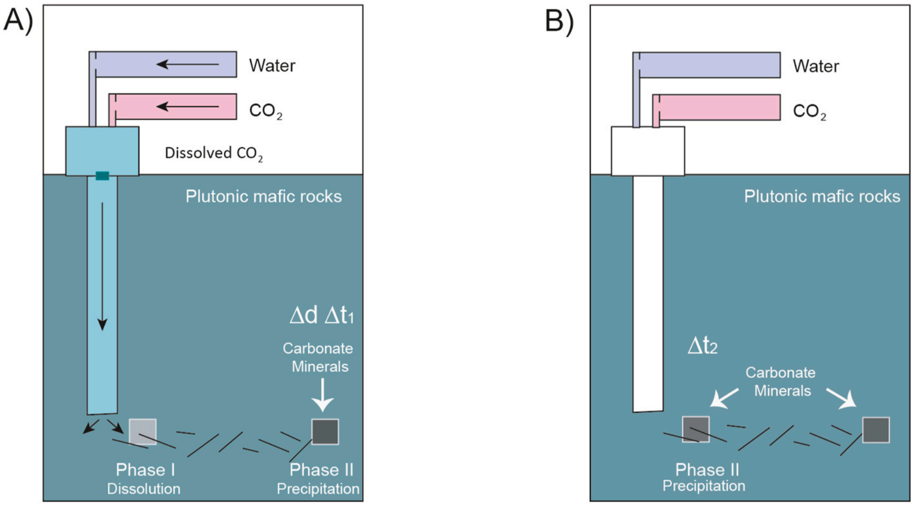

Fig. 13. A) Stage-I and Stage-II can represent a change in conditions due to the increasing distance from the injection zone and elapsed time. B) Stage-II can also take place sometime after the cessation of CO_2 injection.

increased by using crushed rock, demonstrate that the mineral composition of these gabbroic rock massifs is very suitable for intense rock-water-CO_2 interactions, opening perspectives for *ex-situ* mineral carbonation or even “enhanced weathering” CO_2 sequestration techniques, in which these plutonic rock massifs are quarried and crushed to small size grains and made to react with CO_2 in purposely built reactors (ex-situ mineral carbonation) or under natural conditions (enhanced weathering).

5. Conclusions

This study addresses, through laboratory experiments and geochemical modelling, the feasibility of using a plutonic mafic rock to perform CO_2 mineral carbonation. The mafic rock tested was a gabbro-anorthosite specimen from the Torrão - Odivelas Massif (Portugal), with a chemical composition similar to volcanic rocks (basalts) that, in other projects, ensured fast mineral carbonation of CO_2.

The main novelties of the study lies in its experimental approach and the rock type tested. The experimental setup aimed at maintaining realistic conditions in terms of pressure, temperature, and the chemical properties of the injected fluid. Thus, and besides testing plutonic mafic rock that have seldom been the subject mineral carbonation studies, seawater was used instead of ultrapure MilliQ water, and no additives were introduced to reach a pH level adequate for mineral precipitation, as is often done in other laboratory experiments. Instead, we chose to reproduce the evolution of the pH by “ageing” the brine, conducting the experiments in two stages.

(i) In Stage-I, the seawater supersaturated in CO_2, created an acidified environment (pH decrease) that favoured rapid silicate dissolution (Ca^{2+}, Mg^{2+}, SiO_4^{2-} and Al^{3+} increased in the brine) through reaction with crushed rock
(ii) In Stage-II, the “aged” seawater from Stage-I subsaturated in CO_2, still under acidic conditions, resulted in a lower dissolution rate of silicates (lower increase of Ca and Mg and decrease of SiO_2 and Al), and signs of carbonation were detected by SEM-EDS and XRD.

Calcium, magnesium, iron and silica can be used to describe the gabbro-anorthosite dissolution-precipitation. The experimental results were generally reproduced by a geochemical model implemented in *Crunchflow* to simulate the laboratory experiments and extrapolate data for longer time periods. The geochemical model showed a variation of the brine composition that can be explained by the precipitation of new mineral phases, in agreement with the small amounts of detected carbonates, after 90 days.

The very low specific surface of a plutonic specimen does not provide the best environment for large-scale mineral carbonation, as the specific surface is restricted to the secondary porosity provided by fractures. Still, the laboratory experiments and model showed that mineral carbonation does occur on the surface of specimens and that the possibility of using these geological environments for *in situ* mineral carbonation should not be discarded. Further research is being conducted to upscale the results of the geochemical model to the field scale and understand if the carbonation rates in the whole massif are adequate for CO_2 emissions reduction, even if from small CO_2 sources, possibly coupled with hydraulic fracturing to increase the permeability and the reactive surface area around an injection well.

Perhaps even more interesting prospects are provided by the strong CO_2-water-rock interaction observed when using crushed rock in the Stage-I experiment, a robust indication that *ex situ* mineral carbonation or *enhanced weathering* could be achieved with plutonic mafic rocks outcropping in southern Portugal.

Credit author statement

Edgar Berrezueta, Patricia Moita, Jorge Pedro and Julio Carneiro: Conceptualization. **Halidi Abdoulghafour, José Mirao, Massimo Beltrame and Pedro Barrulas**: Methodology, Software. **Edgar Berrezueta, Patricia Moita and Julio Carneiro**: Writing- Original draft preparation. **Alexandre Araújo, Edgar Berrezueta, Luis Lopes and Julio Carneiro**: Resources **Maria Helena Caeiro**: Software, Validation.: **Edgar Berrezueta, Patricia Moita, Halidi Abdoulghafour and Julio Carneiro**: Writing- Reviewing and Editing.

Declaration of competing interest

The authors declare that they have no known competing financial interests or personal relationships that could have appeared to influence the work reported in this paper.

Data availability

Data will be made available on request.

Acknowledgements

This work was supported by national funds through the Portuguese FCT—Fundação Para a Ciência e Tecnologia—in the scope of project INCARBON, contract PTDC/CTA-GEO/31853/2017. The authors thank to the four anonymous reviewers and the editorial committee for their observations and suggestions for improving the manuscript.

References

Abdoulghafour, H., Moitas, P., Berrezueta, E., Pedro, J., Carneiro, J., 2021. Geochemical modeling of CO2-brine gabbro-diorite interaction for in-situ mineral carbonation, 2021. In: Conference Proceedings. 82nd EAGE Annual Conference & Exhibition, pp. 1–5. Oct 2021.
André, L., Audigane, P., Azaroual, M., Menjoz, A., 2007. Numerical modeling of fluid–rock chemical interactions at the supercritical CO2–liquid interface during CO2 injection into a carbonate reservoir, the Dogger aquifer(Paris Basin, France). Energy Convers. Manag. 48, 1782–1797.
Beltrame, M., Liberato, M., Mirão, J., Santos, H., Barrulas, P., Branco, F., Gonçalves, L., Candeias, A., Schiavon, N., Schiavon, N., 2019. Islamic and post Islamic ceramics from the town of Santarém (Portugal): the continuity of ceramic technology in a transforming society. J. Archaeol. Sci. Rep. 23, 910–928.
Berrezueta, E., Kovacs, T., Herrera-Franco, G., Mora-Frank, C., Caicedo-Potosí, J., Carrión-Mero, P., Carneiro, J., 2023. Laboratory studies on CO2-brine-rock interaction: an analysis of research trends and current knowledge. Int. J. Greenh. Gas Control 123, 103842. https://doi.org/10.1016/j.ijggc.2023.103842.
Berrezueta, E., Ordoñez Casado, B., Quintana, L., 2016. Qualitative and quantitative changes in detrital reservoir rocks caused by CO_2 – brine – rock interactions during first injection phases (Utrillas sandstones, northern Spain). Solid Earth 7, 37–53.
Druckenmiller, M.L., Maroto-Valer, M.M., 2005. Carbon sequestration using brine of adjusted pH to form mineral carbonates. Fuel Process. Technol. 86, 1599–1614.
GCCSI, 2021. Report from the Global CCS Institute. https://www.globalccsinstitute.com/resources/global-status-report.
Georgiou, C.D., Sun, H.J., McKay, C.P., Grintzalis, K., Papapostolou, I., Zisimopoulos, D., Panagiotidis, K., Zhang, G., Koutsopoulou, E., Christidis, G.E., margiolaki, I., 2015. Evidence for photochemical production of reactive oxygen species in desert soils. Nat. Commun. 6, 7100.
Gislason, S.R., Oelkers, E.H., 2014. Carbon storage in basalt. Science 344 (6182), 373–374.
Gysi, A.P., Stefánson, A., 2012a. CO2-water-basalt interaction. Low temperature experiments and implications for CO2 sequestration into basalts. Geochem. Cosmochim. Acta 81, 129–152.
Gysi, A.P., Stefánson, A., 2012b. Experiments and geochemical modelling of Co2 sequestration during hydrothermal basalt alteration. Chem. Geol. 306–307, 10–28.
Harrison, A.L., Tutolo, B.A., DePaolo, D.J., 2019. The role of reactive transporting modelling in geologic carbón storage. Elements 15, 24–40.
Hudak, P.F., 1994. Effective porosity of unconsolidated sand; Estimation and impact on capture zone geometry. Environ. Geol. 24, 140–143.
IEA, 2017. Energy Technology Perspectives 2017. Catalysing Energy Technology Transformations. https://www.iea.org/reports/energy-technology-perspectives-2017. (Accessed 14 August 2022).
IEAGHT, 2011. Geological storage of CO2 in basalts. Report:2011/TR2, September 2011. https://ieaghg.org/docs/General_Docs/Reports/2011-TR2.pdf. (Accessed 14 August 2022).
IPCC, 2022. CVS in the Lasted IPCC Report “Migration of Climate Change”. https://www.globalccsinstitute.com/wp-content/uploads/2022/04/CCS-in-the-latest-IPCC-rep

ort-%E2%80%9CMitigation-of-Climate-Change%E2%80%9D-April-2022-1.pdf. (Accessed 14 August 2022).

IPCC, 2011. Summary for policymakers. In: Edenhofer, O., Pichs-Madruga, R., Sokona, Y., Seyboth, K., Matschoss, P., Kadnr, S., Zwickel, T., Eickemeier, P., Hansen, G., Schlömer, S., von Stechow, C.((Eds.), IPCC Special Report on Renewable Energy Sources and Climate Change Mitigation. Cambridge University Press, Cambridge, New York, pp. 1–26. https://www.ipcc.ch/site/assets/uploads/2018/03/Summary-for-Policymakers-1.pdf. (Accessed 14 August 2022).

Jesus, A., Mateus, A., Oliveira, V., Munhá, J., 2003. Ore forming systems in the layered gabbroic sequence of the Beja igneous Complex (Ossa morena zone, Portugal); state of the art and future perspectives. In: Eliopoulos, D.G., others (Eds.), SGA Meeting Mineral Exploration and Sustainable Development, vol. 1. Millpress, Rotterdam, pp. 591–594.

Kelemen, P.B., Matter, J., 2008. *In situ* carbonation of peridotite for CO_2 storage. Proc. Natl. Acad. Sci. USA 105 (45), 17295–17300. https://doi.org/10.1073/pnas.0805794105.

Lacinska, A.M., Styles, M.T., Bateman, K., Hall, M., Brown, P.D., 2017. An experimental study of the carbonation of serpentinite and partially serpentinised peridotites. Front. Earth Sci. 5, 37. https://doi.org/10.3389/feart.2017.00037.

Luquot, L., Gouze, P., 2009. Experimental determination of porosity and permeability changes induced by injection of CO_2 into carbonate rocks. Chem. Geol. 265, 148–159.

Matter, J.M., Stute, M., Snaebjornsdottir, S.O., Oelkers, E.H., Gislason, S.R., Aradottir, E. S., Sigfusson, B., Gunnarsson, I., Sigurdardottir, H., Gunnlaugsson, E., Axelsson, G., Alfredsson, H.A., Wolff-Boenisch, D., Mesfin, K., Fernandez de la Reguera Taya, D., Hall, J., Dideriksen, K., Broecker, W.S., 2016. Rapid carbon mineralization for permanent disposal of anthropogenic carbon dioxide emissions. Science 352 (6291), 1312–1314.

Marieni, C., Oelkers, E., 2018. Carbon sequestration potential of altered mafic reservoirs. Energy Proc. 146, 68–73.

Matter, J.M., Broecker, W.S., Stute, M., Gislason, S.R., Oelkers, E.H., Stefánsson, A., Wolff-Boenisch, D., Gunnlaugsson, E., Axelsson, G., Björnsson, G., 2009. Permanent carbon dioxide storage into basalt: the CarbFix pilot project, Iceland. Energy Proc. 1 (1), 3641–3646.

McGrail, B.P., Spane, F.A., Amonette, J.E., Thompson, C.R., Brown, C.F., 2014. Injection and monitoring at the Wallula basalt pilot project. Energy Proc. 63, 2939–2948.

Moita, P., Berrezueta, E., Abdoulghafour, H., Beltrame, M., Pedro, J., Mirão, J., Miguel, C., Galacho, C., Sitzia, F., Barrulas, P., Carneiro, J., 2020a. Mineral carbonation of CO_2 in mafic plutonic rocks. II: early-phase SC CO_2-brine-rock interaction. Appl. Sci. 10, 5083.

Moita, P., Berrezueta, E., Pedro, J., Miguel, C., Beltrame, M., Galacho, C., Mirão, J., Araújo, A., Lopes, L., Carneiro, J., 2020b. Experiments on mineral carbonation of CO_2 in gabbro's from the Sines massif-first results from project InCarbon. Comunicações Geológicas 107, 91–96.

Palandri, J., Kharaka, Y., 2004. A Compilation of Rate Parameters of Water-Mineral. Interaction Kinetics for Application to Geochemical Modeling. Geological Survey, Reston, VA, USA, p. 71.

Pedro, J., Araújo, A.A., Moita, P., Beltrame, M., Lopes, L., Chambel, A., Berrezueta, E., Carneiro, J., 2020. Mineral carbonation of CO_2 in Mafic Plutonic Rocks, I – screening criteria and application to a case study in SW Portugal. Appl. Sci. 10, 4879.

Pedro, J., Araújo, A., Fonseca, P., Munhá, J., Ribeiro, A., Mateus, A., 2013. Cinturas Ofiolíticas e Metamorfismo de Alta Pressão no Bordo SW da Zona de Ossa Morena. In: Dias, R., Araújo, A., Terrinha, P. e, Kullberg, J.C. (Eds.), Geologia de Portugal, Volume I, Geologia Pré-mesozóica de Portugal. Escolar Editora, Portugal, pp. 647–671.

Peuble, S., Andreani, M., Gouze, P., Pollet-Villard, M., Reynard, B., Van de Moortele, B., 2017. Multi-scale characteriation of incipient carbonation of peridotite. Chem. Geol. 476, 150–160.

Rosenbauer, R., Koksalan, T., Palandri, J., 2005. Experimental investigation of CO_2-brine-rock interactions at elevated temperature and pressure: implications for CO_2 sequestration in deep-saline aquifers. Fuel Process. Technol. 86, 1581–1597.

Rigopoulos, I., Harrison, A.L., Delimitis, A., Ioannou, I., Efstathiou, A.M., Kyratsi, T., Oelkers, E.H., 2018. Carbon sequestration via enhanced weathering of peridotites and basalts in seawater. Appl. Geochem. 91, 197–207. https://doi.org/10.1016/j.apgeochem.2017.11.001.

Rogers, K.L., Neuhoff, P.S., Pedersen, A.K., Bird, D.K., 2006. CO2 metasomatism in a basalt-hosted petroleum reservoir, Nuusuaq, West Greenland. Lithos 92 (1–2), 55–82.

Sanna, A., Uibu, M., Caramanna, G., Ruusik, R., Maroto-Valer, M.M., 2014. A review of mineral carbonation technologies to sequester CO2. Chem. Soc. Rev. 43, 8049–8080.

Snæbjörnsdóttir, S., Gislason, S.R., Galeczka, I.M., Oelkers, E., 2018. Reaction path modeliing in situ mineralization of CO2 at the carbfix site at Hellisheidi Sw-Iceland. Geochem. Cosmochim. Acta 220, 348–366.

Snæbjörnsdóttir, S., Gislason, S.R., 2016. CO2 storage potential of basaltic rocks off shore Iceland. Energy Proc. 86, 371–380.

Steefel, C.I., 2008. Geochemical kinetics and transport. In: Brantley, S., Kubicki, J., White, A. (Eds.), Kinetics of Water Interaction. Springer, New York, pp. 545–589.

Stockman, G.J., 2012. Experimental Study of Basalt Carbonatization. Geochemistry, 2012. Université Paul Sabatier - Toulouse III, p. 193.

Steefel, C.I., Lasaga, A., 1994. A coupled model for transport of multiple chemical-species and kinetic precipitation dissolution reactions with application to reactive flow in single-phase hydrothermal systems. Am. J. Sci. 294, 529–592.

Steefel, C.I., 2009. *CrunchFlow Software For Modeling Multicomponent Reactive Flow And Transport*; User's Manual; Earth Sciences Division, 2009. National Laboratory: Berkeley, CA, USA, Lawrence Berkeley, pp. 12–91.

Steefel, C.I., Appelo, T., Arora, B., Jacques, D., Kalbacher, T., Kolditz, O., Lagneau, V., Lichtner, P., Mayer, K., Meeussen, J., Molins, S., Moulton, D., Shao, H., Simunek, J., Spycher, N., Yabusaki, S.B., Yeh, G.T., 2014. Reactive transport codes for subsurface environmental simulation. Comput. Geosci. 19, 445–478.

Snæbjörnsdóttir, S., Sigfússon, B., Marieni, C., Goldberg, D., Gislason, S.R., Oelkers, E., 2020. Carbon dioxide storage through mineral carbonation. Nat. Rev. Earth Environ. 1, 90–102.

Sonnenthal, E., Spycher, N., 2001. Drift-Scale Coupled Processes (DST and THC Seepage) Models. United States. https://doi.org/10.2172/837097. (Accessed 14 August 2022).

Tarkowski, R., Wdowin, M., Manecki, M., 2014. Petrophysical examination of CO_2-brine-rock interactions—results of the first stage of long-term experiments in the potential Zaosie Anticline reservoir (central Poland) for CO_2 storage. Environ. Monit. Assess. 187, 4215.

Wells, R.K., Xiong, W., Giammar, D., Skemer, P., 2017. Dissolution and surface roughning of Columbia River flood basal at geological carbon sequestration conditions. Chem. Geol. 467, 100–109.

Wilson, S.A., Raudsepp, M., Dipple, G.M., 2006. Verifying and quantifying carbon fixation in minerals from serpentine-rich mine tailings using the Rietveld method with X-ray powder diffraction data. Am. Mineral. 91, 1331–1341. https://doi.org/10.2138/am.2006.2058.

Wolff-Boenisch, D., Galeczka, I.M., 2018. Flow-through reactor experiments on basalt-(sea) water-CO2 reactions at 90 °C and neutral pH. What happens to the basalt pore space under post-injection conditions? Int. J. Greenh. Gas Control 68, 176–190.

Xu, T., Apps, J.A., Pruess, K., 2004. Numerical simulation of CO_2 disposal by mineral trapping in deep aquifers. Appl. Geochem. 19, 917–936.

Xu, T., Apps, J.A., Pruess, K., 2005. Mineral sequestration of carbon dioxide in a sandstone–shale system. Chem. Geol. 217 (3–4), 295–318.

Zhang, S., DePaolo, D.J., 2017. Rates of CO2 mineralisation in geological carbon storage. Acc. Chem. Res. 50, 2075–2084.